Supporting Information

Carbon Dots embedded CoNi bimetallic phosphides nanorods as efficient electrocatalyst for overall water splitting

Yantong Long[a,b], Guoliang Zhao[b], Liuxin Yang[b], Yongjun Xu[a*], Chen Xu[b*]

[a] School of Chemistry and Chemical Engineering, Harbin Institute of Technology, Harbin 150001, China

[b] Institute of Materials, China Academy of Engineering Physics, Mianyang 621907, China

[*]Correspondence to: Y. J. Xu (E-mail: xuyongjun1218@126.com) & C. Xu (E-mail: chenxuacademic@163.com)

Details of Density Functional Theory (DFT) Calculations: All the DFT calculations were performed by the Vienna Ab initio Simulation Package (VASP)[1] with the projector augmented wave (PAW) method[2]. The exchange-functional was treated using the generalized gradient approximation (GGA) with Perdew-Burke-Emzerhof (PBE) functional[3]. The energy cutoff for the plane wave basis expansion was set to 400 eV. Partial occupancies of the Kohn-Sham orbitals were allowed using the Gaussian smearing method and a width of 0.2 eV. The Brillourin zone was sampled with Monkhorst mesh of 4×4×4 for the optimization for the bulk structure of CoNi-P/CDs/NF, Co-P/CDs/NF, Ni-P/CDs/NF, CoNi-P/NF. The self-consistent calculations applied a convergence energy threshold of 10^{-5} eV, and the force convergency was set to 0.05 eV/Å.

The free energy corrections were considered at the temperature of 298 K, following:

$$\Delta G = \Delta E + \Delta G_{ZPE} + \Delta G_U - T\Delta S$$

where ΔE, ΔG_{ZPE}, ΔG_U, and ΔS refer to the DFT calculated energy change, the correction from zero-point energy, the correction from inner energy and the correction from entropy[4].

The solvent effect was considered due to the stabilization of adsorbate from the H-bond network in the water. A stabilization of -0.30 and -0.30 were considered for OH* and OOH*[5, 6].

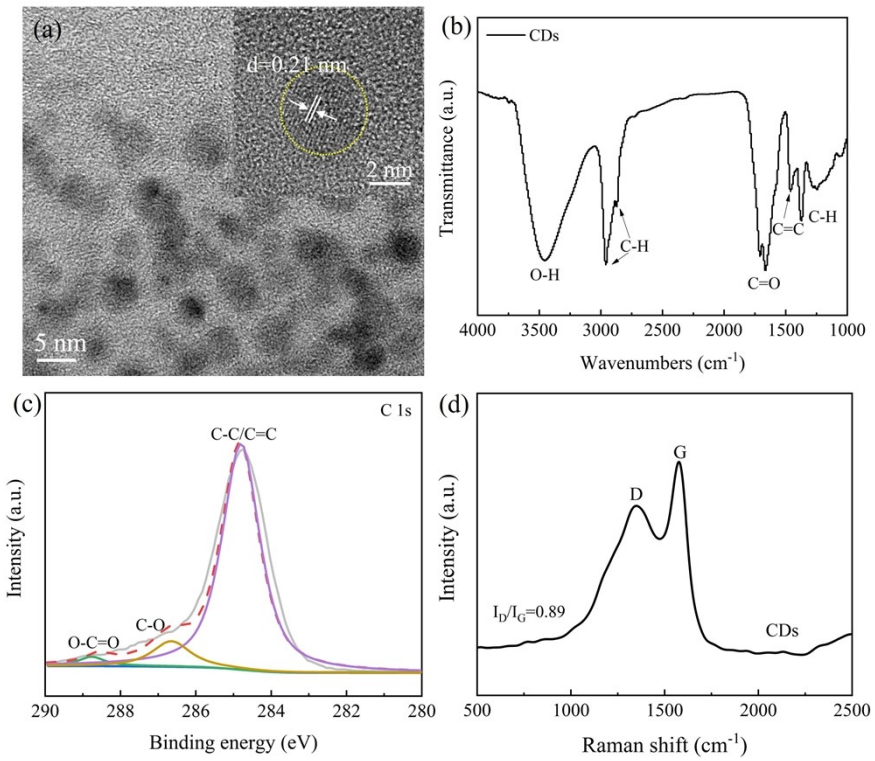

Fig. S1. (a) TEM image of CDs, (b) FT-IR spectra of CDs, (c) XPS spectra of C 1s, (d) Raman spectra of CDs.

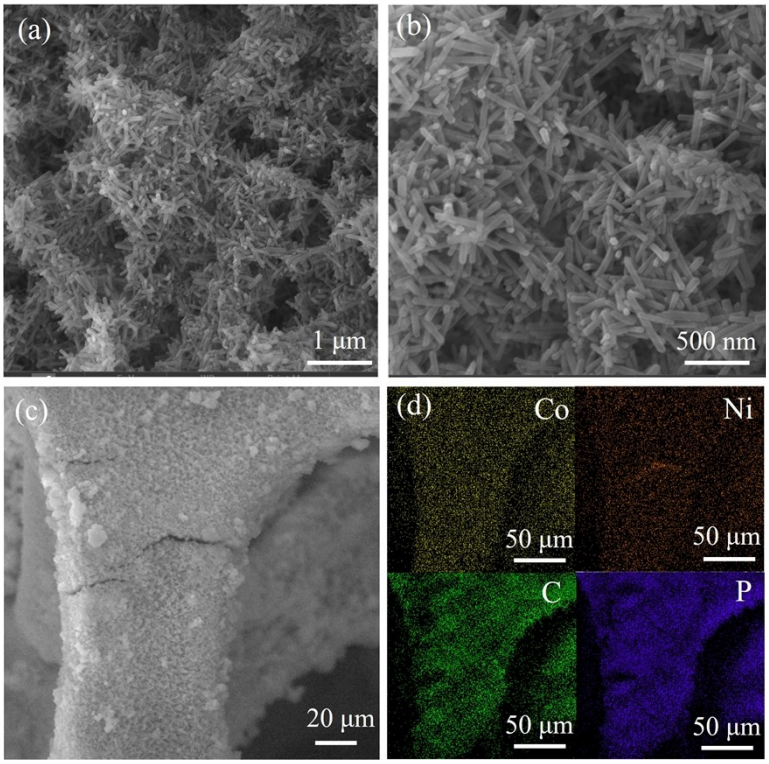

Fig. S2. (a-c) SEM images of CoNi-P/CDs/NF, (d) corresponding EDX elemental maps: Co (yellow), Ni (orange), C (green) and P (blue).

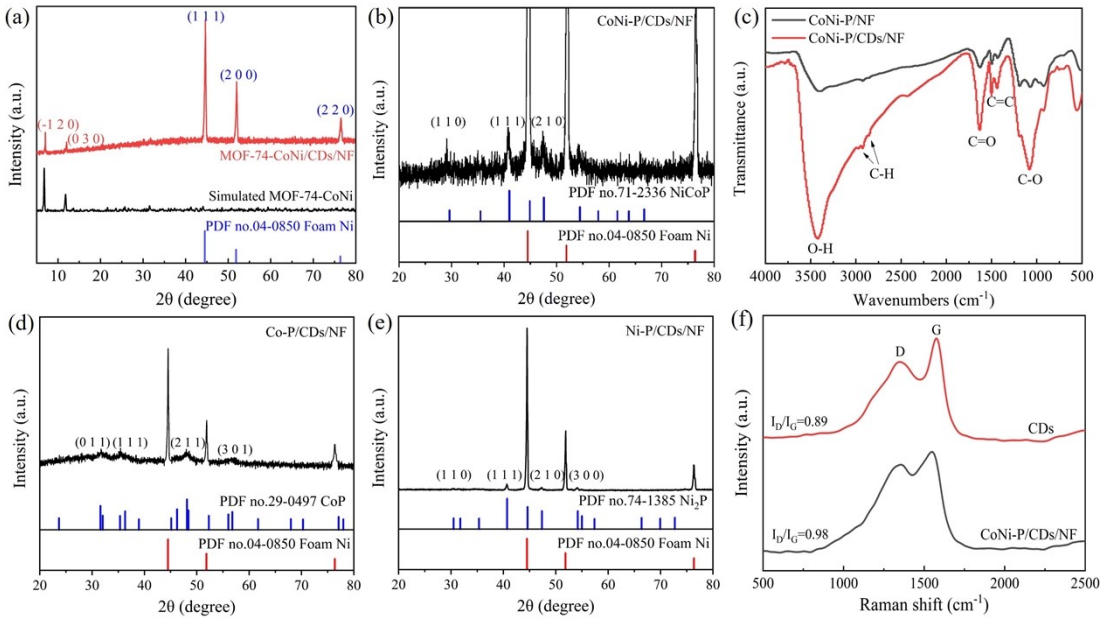

Fig. S3. XRD patterns of (a) MOF-74-CoNi/CDs/NF, (b) CoNi-P/CDs/NF, (c) FT-IR spectra of CoNi-P/CDs/NF and CoNi-P/NF, XRD pattern of (d) Co-P/CDs/NF, (e) Ni-P/CDs//NF, (f) Raman spectra of CDs and CoNi-P/CDs/NF.

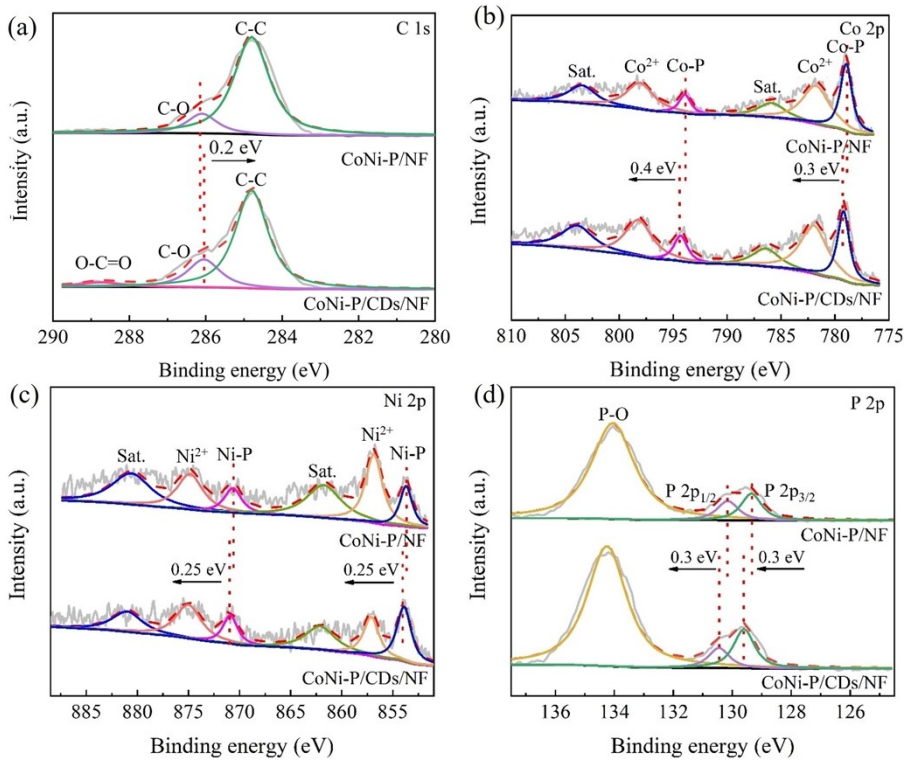

Fig. S4. (a) C 1s, (b) Co 2p, (c) Ni 2p and (d) P 2p XPS comparison between CoNi-P/CDs/NF and CoNi-P/NF.

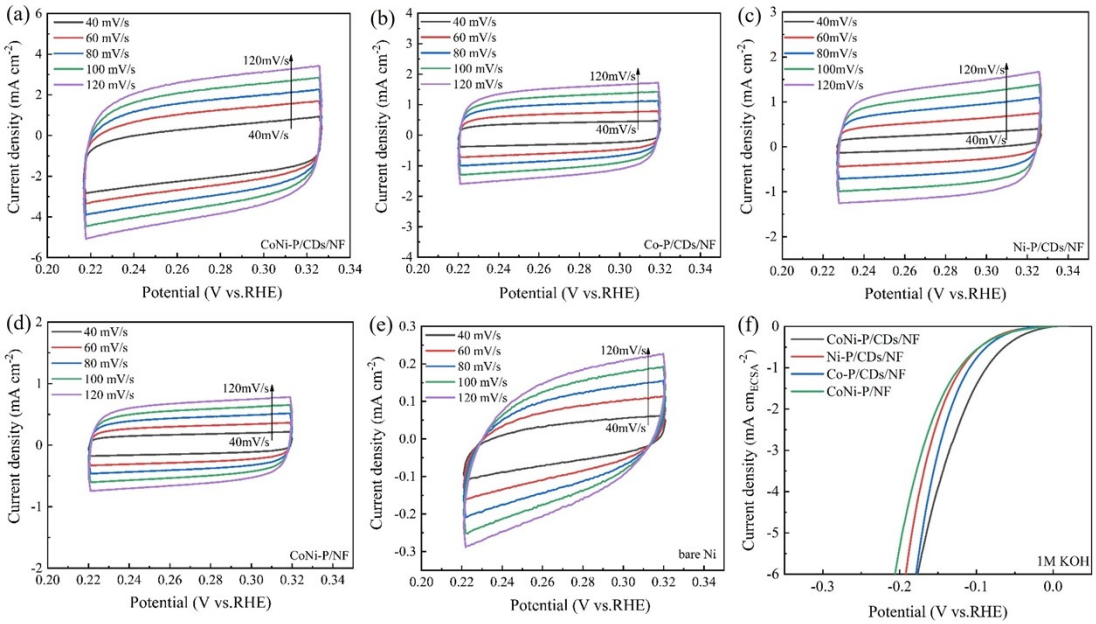

Fig. S5. Cyclic voltammograms of (a) CoNi-P/CDs/NF, (b) Co-P/CDs/NF, (c) Ni-P/CDs/NF, (d) CoNi-P/NF and (e) bare Ni electrodes recorded in the non-Faradaic potential region (0.22-0.32 V vs. RHE) at different scan rates (40, 60, 80, 100, and 120 mV/s) toward HER in 1M KOH. (f) ECSA-normalized LSV curves of CoNi-P/CDs/NF, Co-P/CDs/NF, Ni-P/CDs/NF and CoNi-P/NF in 1M KOH.

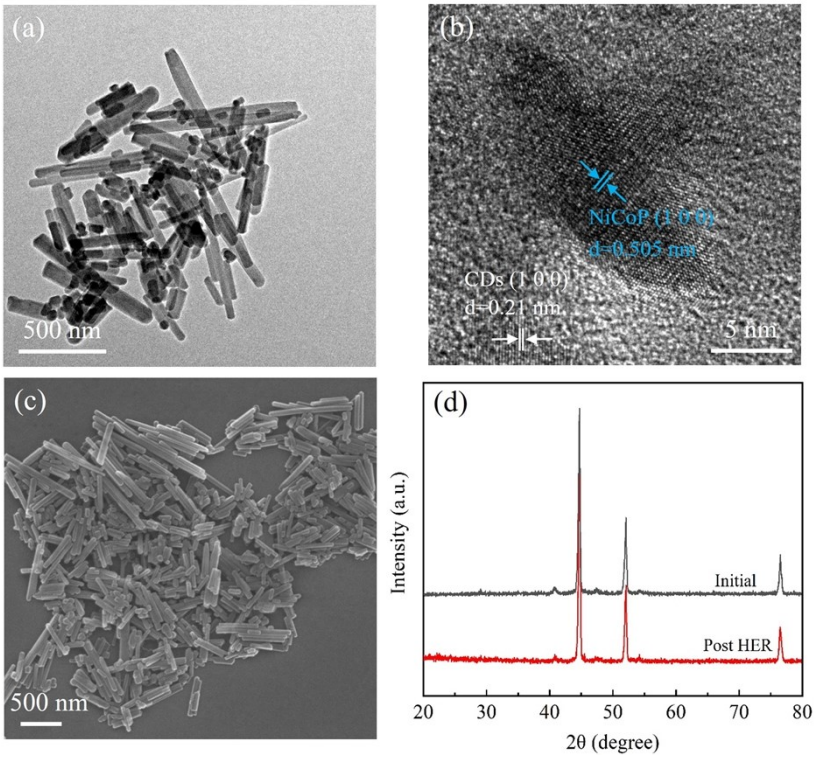

Fig. S6. (a) TEM image of CoNi-P/CDs/NF after HER electrolysis. (b) high-resolution TEM images of CoNi-P/CDs/NF after HER electrolysis. (c) SEM image of CoNi-P/CDs/NF after HER electrolysis. (d) XRD pattern of CoNi-P/CDs/NF before and after HER electrolysis.

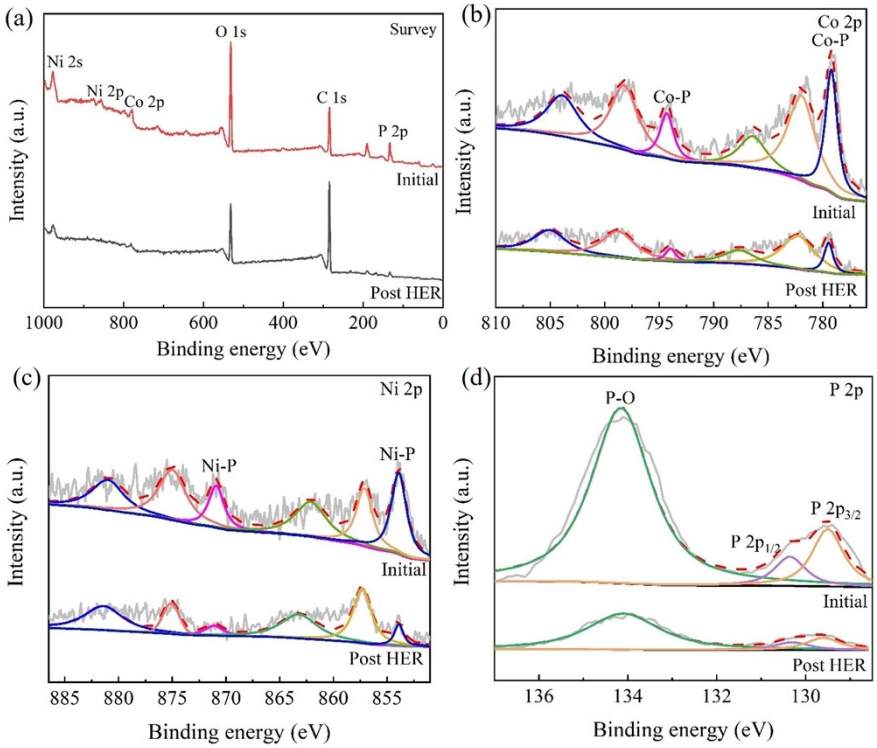

Fig. S7. (a) Survey, (b) Co 2p, (c) Ni 2p and (d) P 2p of CoNi-P/CDs/NF spectrums before and after HER test.

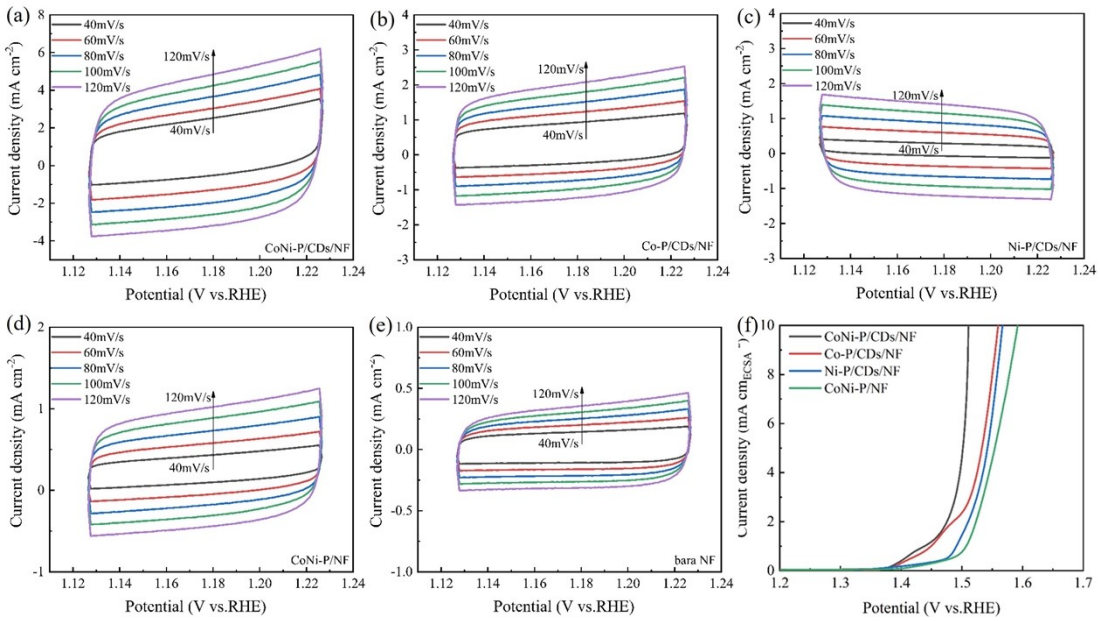

Fig. S8. Cyclic voltammograms of (a) CoNi-P/CDs/NF, (b) Co-P/CDs/NF, (c) Ni-P/CDs/NF (d) CoNi-P/NF and (d) bare NF electrodes recorded in the non-Faradaic potential region (1.13-1.23 V vs. RHE) at different scan rates (40, 60, 80, 100, and 120 mV/s) toward OER in 1M KOH. (f) ECSA-normalized LSV curves of CoNi-P/CDs/NF, Co-P/CDs/NF, Ni-P/CDs/NF and CoNi-P/NF in 1M KOH

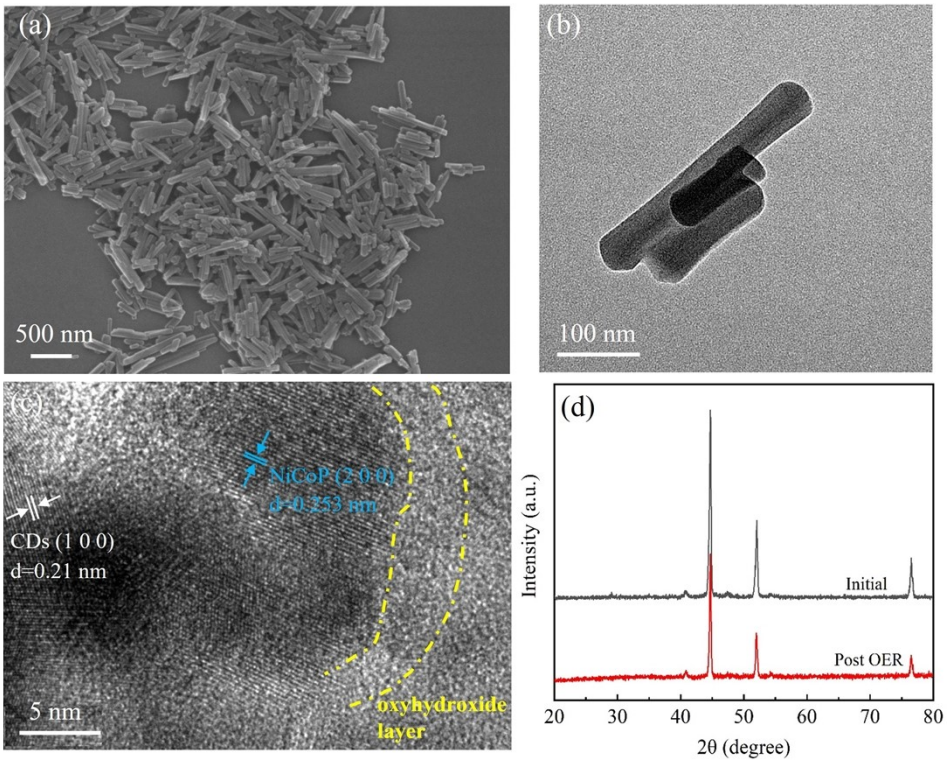

Fig. S9. (a) SEM image of CoNi-P/CDs/NF after OER electrolysis, (b) TEM image of CoNi-P/CDs/NF after OER electrolysis, (c) high-resolution TEM images of CoNi-P/CDs/NF after OER electrolysis, (d) XRD pattern of CoNi-P/CDs/NF before and after OER electrolysis.

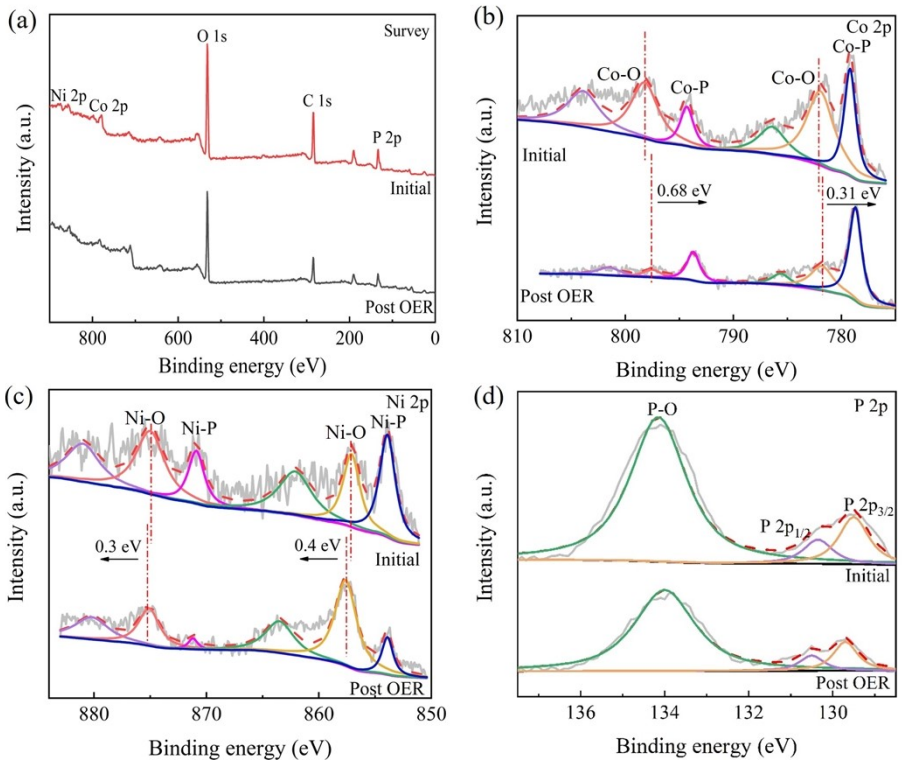

Fig. S10. (a) Survey, (b) Co 2p, (c) Ni 2p and (d) P 2p of CoNi-P/CDs/NF spectrums before and after OER test.

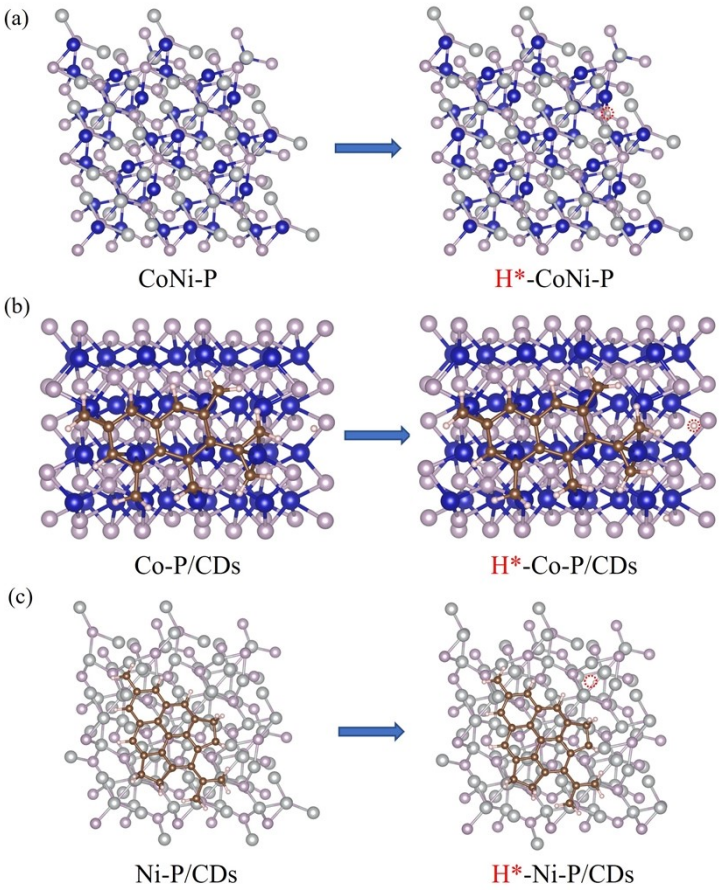

Fig. S11. HER pathways of (a) CoNi-P (b) Co-P/CDs (c) Ni-P/CDs.

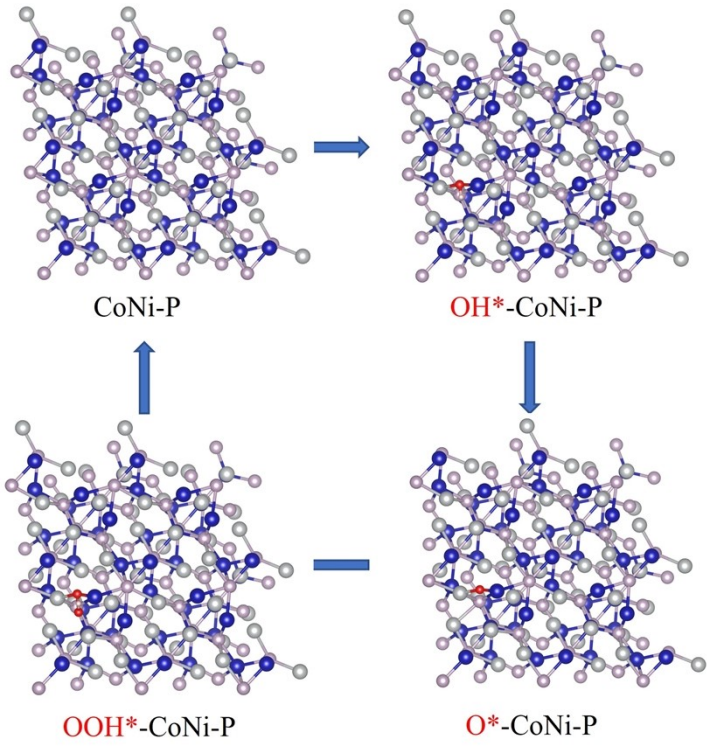

Fig. S12. OER pathways of CoNi-P.

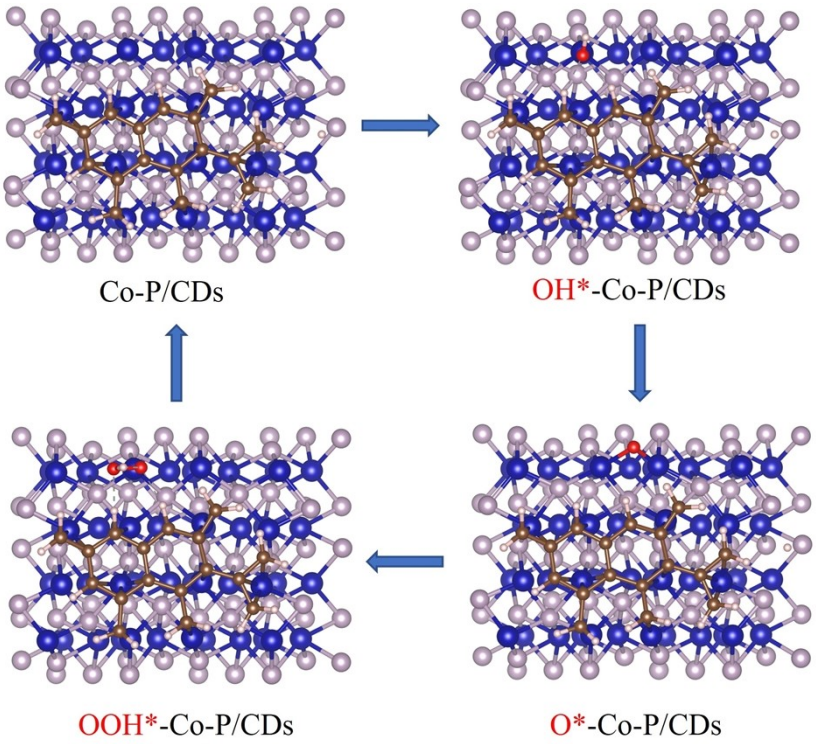

Fig. S13. OER pathways of Co-P/CDs.

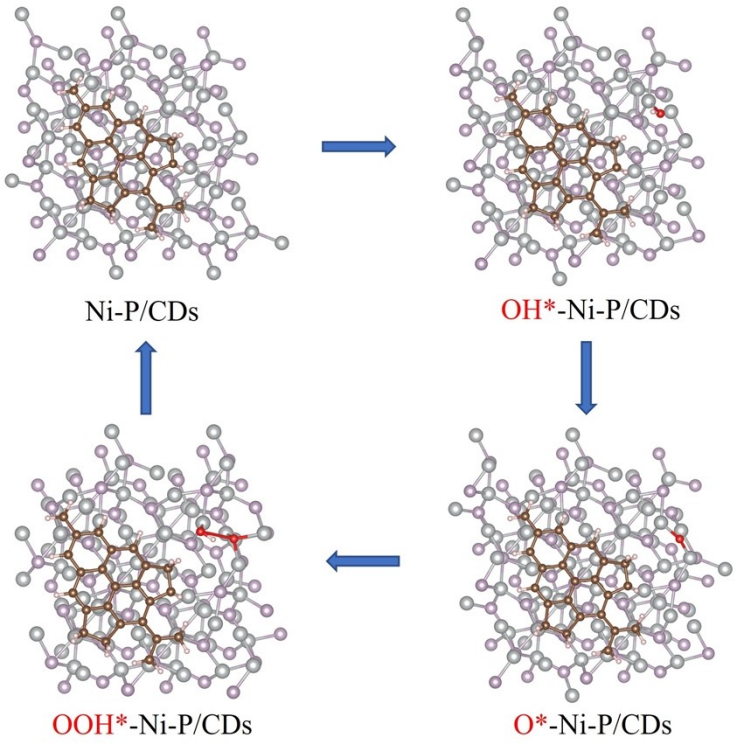

Fig. S14. OER pathways of Ni-P/CDs.

Table S1. Comparison of HER performance of CoNi-P/CDs/NF with other reported highly active HER electrocatalysts in 1 M KOH.

Catalysts	Overpotential (mV at 10 mA cm^{-2})	Reference
CoNi-P/CDs/NF	45.2	This work
NCQDs-100/CoMo/NF	65	Electrochim. Acta 438 (2023) 141595
CFP/$NiCo_2O_4$/CuS	72.3	Mater. Lett. 264 (2020) 127400.
CoP-NCDs/NF	103	Carbon 182 (2021) 327e334
V-CoP@a-CeO_2/CC	68	Adv. Funct. Mater. 30 (2020) 1909618.
Ni_3S_2@Ni	82	J. Eng. Chem. 46 (2020) 178-186.
FQD/CoNi-LDH/NF	150	Chem. Eng. J. 390 (2020) 124525
CoP NFs	95	ACS Catal. 10 (2019) 1-6.
$Co_{0.75}Ni_{0.25}Se$/NF	269	Nanoscale 11 (2019) 7959-7966.
Mo-$CoSe_2$ NS/NF	89	Chem. Eng. J. 47 (2021) 128055.

Table S2. Comparison of OER performance of CoNi-P/CDs/NF with other reported highly active OER electrocatalysts in 1 M KOH.

Catalysts	Overpotential (mV at 10 (20) mA cm^{-2})	Reference
CoNi-P/CDs/NF	184.8	This work
NCQDs-100/CoMo/NF	370	Electrochim. Acta 438 (2023) 141595.
CoNiP/NF	234	Appl. Surf. Sci. 569 (2021) 150762.
Ni-Mo-S@CC	320	Chem. Eur. J. 26 (2020) 4097-4103.
P-SO_3-CDs/NiFe LDH	200	Chem. Eng. J. 420 (2021) 129690.
CoP-NCDs/NF	226	Carbon 182 (2021) 327e334.
V-CoP@a-CeO_2/CC	225	Adv. Funct. Mater. 30 (2020) 1909618.
Ni_3S_2@Ni	310	J. Eng. Chem. 46 (2020) 178-186.
Ni-MoO_2/NF	246	Adv. Funct. Mater. 31 (2021) 2009580.
FQD/CoNi-LDH/NF	340	Chem. Eng. J. 390 (2020) 124525.

Table S3. Comparison of water splitting performance of CoNi-P/CDs/NF with other reported highly active bifunctional electrocatalysts in 1 M KOH.

Catalysts	Overpotential (V at 10 (20) mA cm^{-2})	Reference
CoNi-P/CDs/NF	1.50	This work
CoP-NCDs/NF	1.55	Carbon 182 (2021) 327e334
V-CoP@a-CeO_2/CC	1.56	Adv. Funct. Mater. 30 (2020) 1909618.
Ni_3S_2@Ni	1.61	J. Eng. Chem. 46 (2020) 178-186.
NiCoP@NiMnLDH/NF	1.52	ACS Appl. Mater. Inter, 12 (2019) 4385.
FQD/CoNi-LDH/NF	1.59	Chem. Eng. J. 390 (2020) 124525.
RhCu NTs/CP	1.64	Adv. Eng. Mater. 10 (2020) 1903038.
Mo-$CoSe_2$ NS/NF	1.54	Chem. Eng. J. 47 (2021) 128055.
$Co_{0.75}Ni_{0.25}Se$/NF	1.60	Nanoscale 11 (2019) 7959-7966.
CoP NFs	1.65	ACS Catal. 10 (2019) 1-6.

References:

[1] G. Kressea, J. Furthmüllerb, Efficiency of ab-initio total energy calculations for metals and semiconductors using a plane-wave basis set. Comput. Mater. Sci. 6 (1996) 15-50.

[2] P. E. Blöchl, Projector augmented-wave method. Phys. Rev. B, 50 (1994) 17953.

[3] J. P. Perdew, J. A. Chevary, S. H. Vosko, K. A. Jackson, M. R. Pederson, D. J. Singh, C. Fiolhais, Atoms, molecules, solids, and surfaces: Applications of the generalized gradient approximation for exchange and correlation. Phys. Rev. B, 46 (1992) 6671.

[4] X. Cao, R. Burch, C. Hardacre, P. Hu, An understanding of chemoselective hydrogenation on crotonaldehyde over Pt (1 1 1) in the free energy landscape: The microkinetics study based on first-principles calculations. Catal. Today, 165 (2011) 71-79.

[5] C. Guo, X. Fu, J. Xiao, Theoretical insights on the synergy and competition between thermochemical and electrochemical steps in oxygen electroreduction. J. Phys. Chem. C, 124 (2020). 25796-25804.

[6] H. Xu, D. Cheng, D. Cao, X. Zeng, A universal principle for a rational design of single-atom electrocatalysts. Nat. Catal. 1 (2018) 339-348.